

RESEARCH PAPER

Effect of Composition Electrolyte on the Morphology and Photo Catalytic Activity of Anodized Titanium Nanoporous

Mohamad Mohsen Momeni*

Department of Chemistry, Isfahan University of Technology, Isfahan, Iran

ARTICLE INFO

Article History:

Received 22 September 2018

Accepted 06 November 2018

Published 01 January 2019

Keywords:

Anodizing

Film, Nanotube

Morphology

Nanoporous

Photo catalytic

ABSTRACT

The morphology of titanium dioxide and titanium dioxide-tungsten trioxide nanocomposite films fabricated by anodizing in a glycerol solution containing 0.13 M NH_4F and different quantity of Na_2WO_4 was investigated as a function of sodium tungstate concentrations. The effects of sodium tungstate concentration on the surface morphology were observed by scanning electron microscopy (SEM). It was clearly seen that highly ordered titanium dioxide nanotube array films were formed in an anodizing solution free of tungsten. With a gradual increase in the sodium tungstate concentration, these nanotube structures changed to nanohoneycombs, nanoporous and compact films without porosity. These findings indicate that the composition of anodizing bath is very important factor in determining the surface and structure of anodized films. UV-Visible spectroscopy data show that the band gap decrease with increasing sodium tungstate from 3.23 eV for bare titanium dioxide to 2.78 eV for titanium dioxide-tungsten trioxide nanocomposites. Photo catalytic activity of samples was evaluated by measuring the degradation of methylene blue dye under visible light irradiation. Results revealed that nanocomposite films have excellent photo catalytic performance.

How to cite this article

Momeni M. Effect of Composition Electrolyte on the Morphology and Photo Catalytic Activity of Anodized Titanium Nanoporous. J Nanostruct, 2019; 9(1):154-162. DOI: 10.22052/JNS.2019.01.017

INTRODUCTION

In the past few years, high surface area titanium dioxide nanostructures have attracted much attention for their potential use in several practical applications requiring an interconnected and large internal surface area [1]. More recently, titanium dioxide nanostructures with different sizes and various geometrical shapes were prepared using various physical and chemical synthesis routes such as sol-gel, template synthesis, hydrothermal process and anodizing [2-6]. As an effective fabrication method, the electrochemical anodizing process is useful because of its low cost, large area fabrication, good mechanical adhesion, and electrical conductivity due to the nanotubes being directly connected to the substrate, while the morphology of these anodic films must be adjusted

by controlling the anodic conditions, such as the applied voltage, electrolyte composition, the pH of the electrolyte, duration, and magnetic agitation [1]. Especially, the composition of the electrolyte is an important factor during anodization.

Titanium dioxide nanostructures prepared via anodization of titanium foil possess high surface-to-volume ratios, which are often considered to be advantageous for applications requiring efficient surface reactivity [4-6]. However, previous studies on the applications of titanium dioxide nanostructures have found that the high recombination rate of photo-generated electron-hole pairs and wide band gap were the main drawbacks that limited the photo catalytic activity and visible light response of titanium dioxide nanotube [4]. In order to increase the utilization

* Corresponding Author Email: mm.momeni@cc.iut.ac.ir

efficiency of titanium dioxide on solar energy, researchers do a lot of works from decreasing the band-gap of titanium dioxide and suppressing the recombination of electrons and holes [4, 6]. An efficient approach is to composite titanium dioxide with some special semiconductors which can enhance interfacial electrons transfer to the underlying metal substrate [7-9]. Titanium dioxide-tungsten trioxide nanocomposite has generated considerable interests as a photo catalyst showing optical response in the visible region. Different methods were used to prepare these nanocomposites, but most of these methods were multistage, time consuming and expensive with weak reproducibility. Therefore, a simple, facile, and inexpensive method of synthesizing Titanium dioxide-tungsten trioxide is necessary.

In the present work, we performed the anodizing process in a glycerol solution containing different concentration of Na_2WO_4 and changes in anodized titanium surface morphology was detected using SEM. Herein, a facile, convenient and low-cost method was used to synthesize titanium dioxide-tungsten trioxide nanocomposite by a single-step anodizing of titanium substrate in a non-aqueous bath. A great deal of research has been directed towards using coupled WO_3 - TiO_2 systems with the purpose of promoting the photonic efficiency of TiO_2 . Tungsten has a high charge state with six electrons in the outer orbit

and its ionic radius was 0.60 \AA and was similar to Ti^{4+} (0.605 \AA), thus tungsten atom could substitute easily the titanium atom in TiO_2 lattice [10-12]. WO_3 is a semiconductor with a band gap of 2.8 eV , which is activated by visible light illumination [13]. The basic disadvantage of WO_3 as a photo catalyst is its low photonic efficiency [14]. A schematic of the pretreatment method of titanium sheets and process of producing different films on titanium is shown in Fig. 1. The photo catalytic behaviors were evaluated using measuring the degradation of methylene blue dye under visible light irradiation.

MATERIALS AND METHODS

All chemicals were of analytical grade without further purifying before experiment and solutions were prepared with distilled water.

Titanium dioxide-tungsten trioxide nanocomposites were synthesized by anodic oxidation of titanium in a mixture electrolyte, which was mixing glycerol and NH_4F , followed by the dissolution different concentrations of sodium tungstate. Prior to anodizing, a piece of titanium sheet (99.99% purity, 1-mm thick) was cut into desired dimension and the titanium electrodes was first mechanically polished with different emery type abrasive papers (with the following grades: 80, 240, 800, 1200, and 2400), rinsed in a bath of distilled water, and then chemically etched by immersing in a mixture of HF and HNO_3 acids for

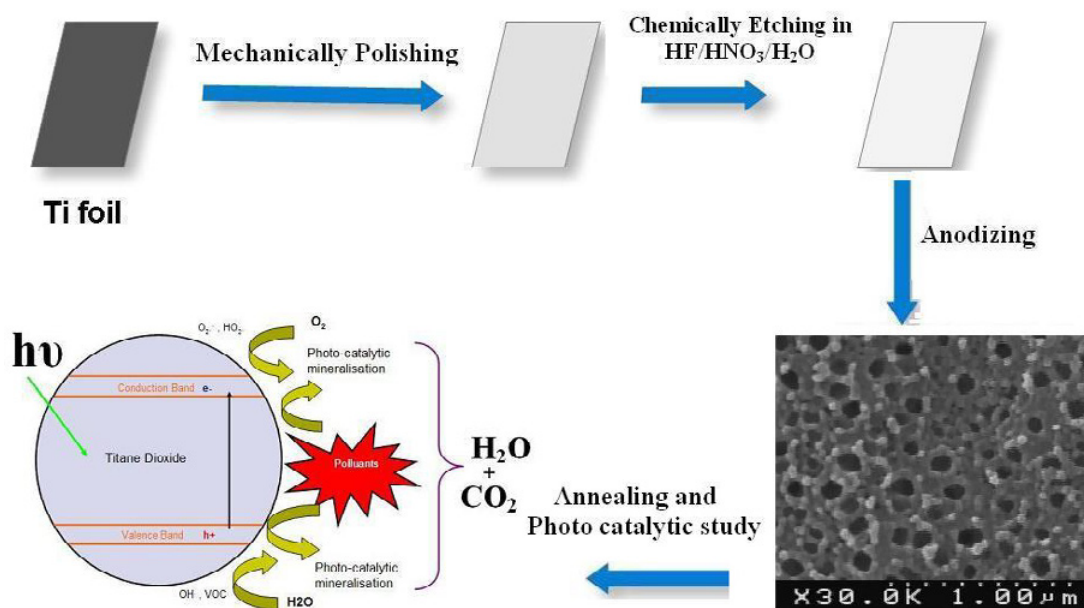


Fig. 1. Schematic presentation of the pretreatment method of titanium sheets and process of producing nanocomposite films on titanium foils.

Table 1. Experimental conditions for 5 different samples.

Samples	Anodizing solution	Anodizing condition
A	98 mL glycerol + 2 ml H ₂ O + 0.13 M NH ₄ F	60 V, 6 h, Room temperature
B	98 mL glycerol + 2 ml H ₂ O + 0.13 M NH ₄ F + 0.6 mM Na ₂ WO ₄ ·2H ₂ O	60 V, 6 h, Room temperature
C	98 mL glycerol + 2 ml H ₂ O + 0.13 M NH ₄ F + 1.2 mM Na ₂ WO ₄ ·2H ₂ O	60 V, 6 h, Room temperature
D	98 mL glycerol + 2 ml H ₂ O + 0.13 M NH ₄ F + 1.8 mM Na ₂ WO ₄ ·2H ₂ O	60 V, 6 h, Room temperature
E	98 mL glycerol + 2 ml H ₂ O + 0.13 M NH ₄ F + 2.4 mM Na ₂ WO ₄ ·2H ₂ O	60 V, 6 h, Room temperature

30 second. The ratio of components HF/HNO₃/H₂O in the mixture was 1:4:5 in volume. The last step of pretreatment was rinsing with distilled water. The anodizing experiments were carried out using a two-electrode system with titanium foil as anode and platinum foil as cathode, respectively. A controlled DC power source (ADAK, PS405) supplied the required constant voltage. Anodizing was carried out in mentioned solutions under a constant voltage of 60 V for 6 h at room temperature. A schematic representation of the anodizing setup is shown in Fig. 2. After anodizing at constant potential, the as-formed samples were annealed in the air at 400 °C for 2 h (1 °C/min) to obtain crystalline nanocomposite. In the present work, we compare the photo catalytic performance of different films with different

quantity of tungsten referred to as A-E. Table 1 summarizes the experimental conditions for 5 different samples.

The surface morphology of all samples were characterized by field emission scanning electron microscopy (FE-SEM, Hitachi S-4160, Japan), and the elemental composition was estimated by energy dispersive X-ray spectroscopy (EDX). The crystalline phases were identified by XRD (Philips X'Pert). Diffraction patterns were recorded in the 2θ range from 20 to 80° at room temperature. The optical absorption of the samples was determined using a diffuse reflectance UV-visible (UV-Vis) spectrophotometer (JASCO V-570). The values of the band gap energy (E_g) were calculated using following equation:

$$(\alpha h\nu) = A(h\nu - E_g)^n \quad (1)$$

where E_g is the band gap energy, h is Planck's constant, ν is the frequency of vibration, $h\nu$ is the incident photon energy, A is a proportional constant and α is the absorption coefficient per unit length [8]. The band gap values were determined by extrapolating the linear region of the plot to $h\nu = 0$.

Photo catalytic activity of all the samples were evaluated by degradation of the aqueous methylene blue (MB) under visible light irradiation. The photo catalytic reaction was carried in a single-compartment cylindrical quartz reactor. A 200 W xenon lamp was used as a light source with a 420 nm cutoff filter to provide visible light. The luminous intensity of the xenon lamp was 100 mW/cm². Light was transmitted by the quartz glass as the xenon lamp shone on the samples. A fan was used to cool down the reactor tube. The actual experiments were performed at room temperature. The initial concentration of methylene blue was 2 mg/L. The volume of the solution was 50 mL. Prior to illumination, the photo catalyst sample was immersed in quartz reactor containing methylene blue and magnetically stirred for 2 h in the dark to ensure

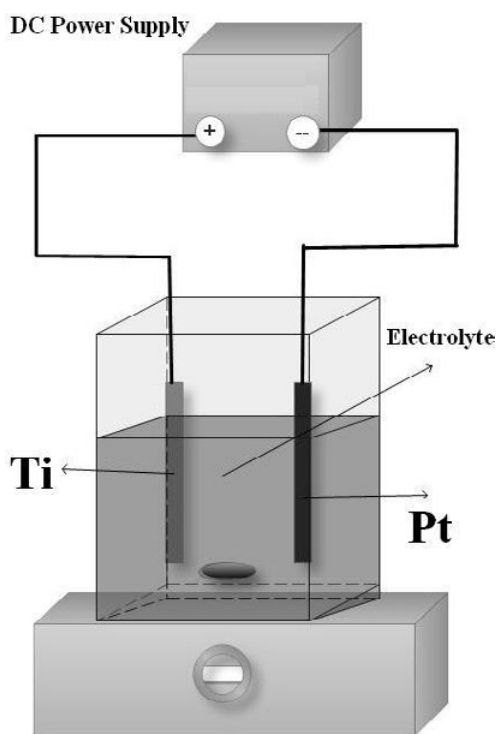


Fig. 2. Schematic representation of the anodizing setup.

the establishment of an adsorption-desorption equilibrium between the photo catalyst and methylene blue. Then the solution was exposed to visible light irradiation under magnetic stirring for 2 h. At each 10 min intervals, 5 ml solution was sampled and the absorbance of methylene blue was measured by a UV-Vis spectrophotometer.

RESULTS AND DISCUSSION

Anodizing is an electrolytic process that creates a protective or decorative oxide film over a metallic surface. In anodizing of titanium, the outer anodic layer (partly exposed to the electrolyte) has an excess of hydroxyl ions compared to the inner layer and is considered to be Ti(OH)_4 . The inner layer, where the de-hydroxylation of the film (water releasing) has occurred, is represented as TiO_2 . In reality there is likely to be a concentration gradient across the film, which can be written as $\text{TiO}_2 \cdot x\text{H}_2\text{O}$, to represent the inner (dry) and outer (hydrated) anodic oxide. The reactions which occur at the anode are:

(i) Oxidation of the metal which releases Ti^{4+} ions and electrons, Eq. (2):



(ii) Combination of Ti^{4+} ions with OH^- and O_2^- species provided by the water.

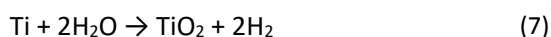
Equations (3) and (4) below account for the hydrated anodic layer and the oxide layer. Further oxide is produced when the hydrated anodic layer releases water by a condensation reaction, Eq. (5):



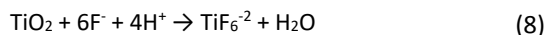
At the cathode there is hydrogen evolution, Eq. (6):



By summing the equations from (2) to (6), the overall process of oxide formation is given:

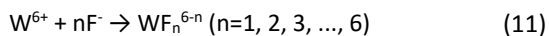


Furthermore, the fluorine ions can attack the hydrated layer and the oxide, as described in the Eqs (8) and (9), or react with Ti^{4+} , Eq. (10), the ions being mobile in the anodic layer, under the high applied electric field:



Clearly, the competition between formation of the oxide (see Eqs. 3-5) and its dissolution (see Eqs. 8-10), is the key factor in determining the anodic titanium oxide structure produced [8].

In electrolyte containing sodium tungstate, in addition to the above reactions, the following reaction (coordination reaction between W^{6+} and F^- ions) could be done:



Equation (11) is the coordination reaction between tungsten ions and fluorine ions. When sodium tungstate was added to anodizing solution, the coordination of W^{6+} and F^- decreased the concentration of free fluorine ions (F^-). Therefore the chemical dissolution becomes slower with the increase of sodium tungstate concentration, leading to the nonuniform formation of nanotubes or a compact film. So it can be said that an optimum concentration of sodium tungstate is required. Because this complex (WF_n^{6-n} is negatively charged, it can move to the positive terminal (anode), where electrochemical oxidation of titanium occurs, and there it can penetrate in the structure of nanotubes.

Fig. 3 shows top-view FE-SEM images of different samples which clearly show formation of various films on the surface of titanium. In Fig. 3a and 3b, different samples displayed nanotube arrays that the surface of them was open. In Fig. 3a, highly ordered and vertically aligned nanotubes were formed on the titanium substrate. The average pore diameter of these nanotubes as calculated from SEM images is 90-100 nm and wall thickness is 20-25 nm. In Fig 3b, a combined structure of nanotubes and nanohoneycombs were formed. It can be seen that nanoparticles are distributed on the surface of these nanostructures. The internal diameter of the tubes is around 50-90 nm. In Fig 3c, a combined structure of nanotubes and nanoporous were formed. It seems on the surface of the nanotubes, a porous structure is emerging. In Fig. 3d and 3e, no nanostructure formed. Compact films, without porosity, were formed on

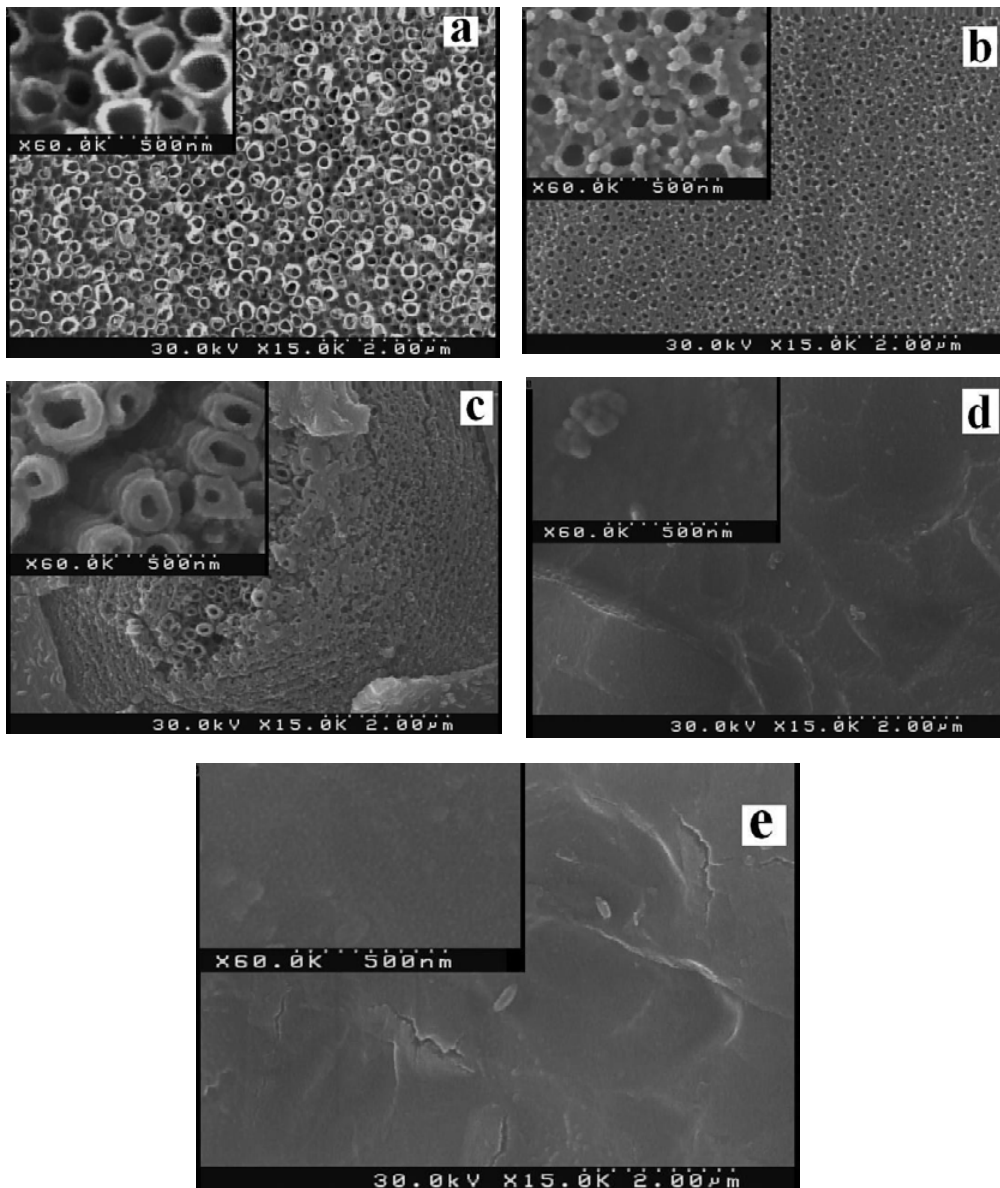


Fig. 3. SEM top-view images of bare titanium dioxide and titanium dioxide-tungsten trioxide nanocomposite samples; a: Sample A, b: Sample B, c: Sample C, d: Sample D and e: Sample E.

the surface of titanium. It can be said that when sodium tungstate concentration in anodizing solution increased to 1.8 mM, surface is covered with a dense film and then not created any regular nanostructures, implying that composition of anodizing bath is a very important factor in determining the surface and structure of anodized layers

The XRD patterns of the bare titanium dioxide and titanium dioxide-tungsten trioxide samples are shown in Fig. 4. Diffractions that are attributable to anatase TiO_2 are clearly observed

in the calcinated sample. The Ti peaks were due to the titanium substrate. XRD pattern of titanium dioxide-tungsten trioxide sample show the diffraction peaks of both WO_3 and TiO_2 and two diffraction peaks of WO_3 are found in this sample.

In addition to XRD analysis, EDX spectra of all films were examined and results present in Fig. 5. It was seen that the films mainly consisted of Ti, O and W. The analysis revealed that the surface present similar composition with presence of titanium as a main energy ($E = 4.5$ kV, W at $E = 1.7$ kV and O at $E = 0.5$ kV that confirms the

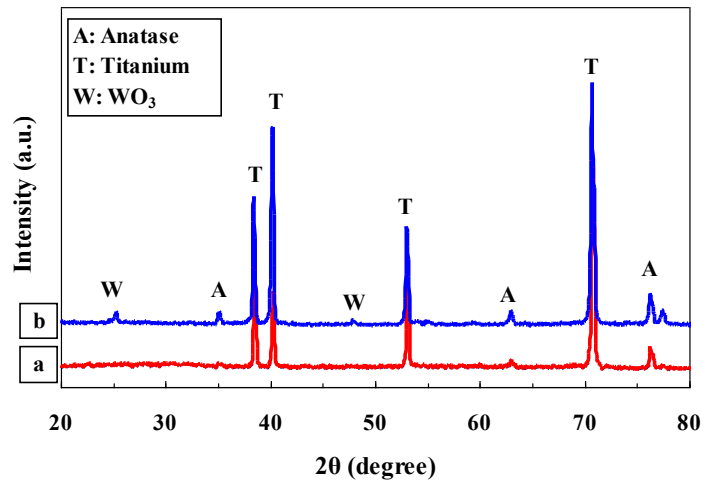


Fig. 4. XRD pattern of bare titanium dioxide and titanium dioxide-tungsten trioxide films.

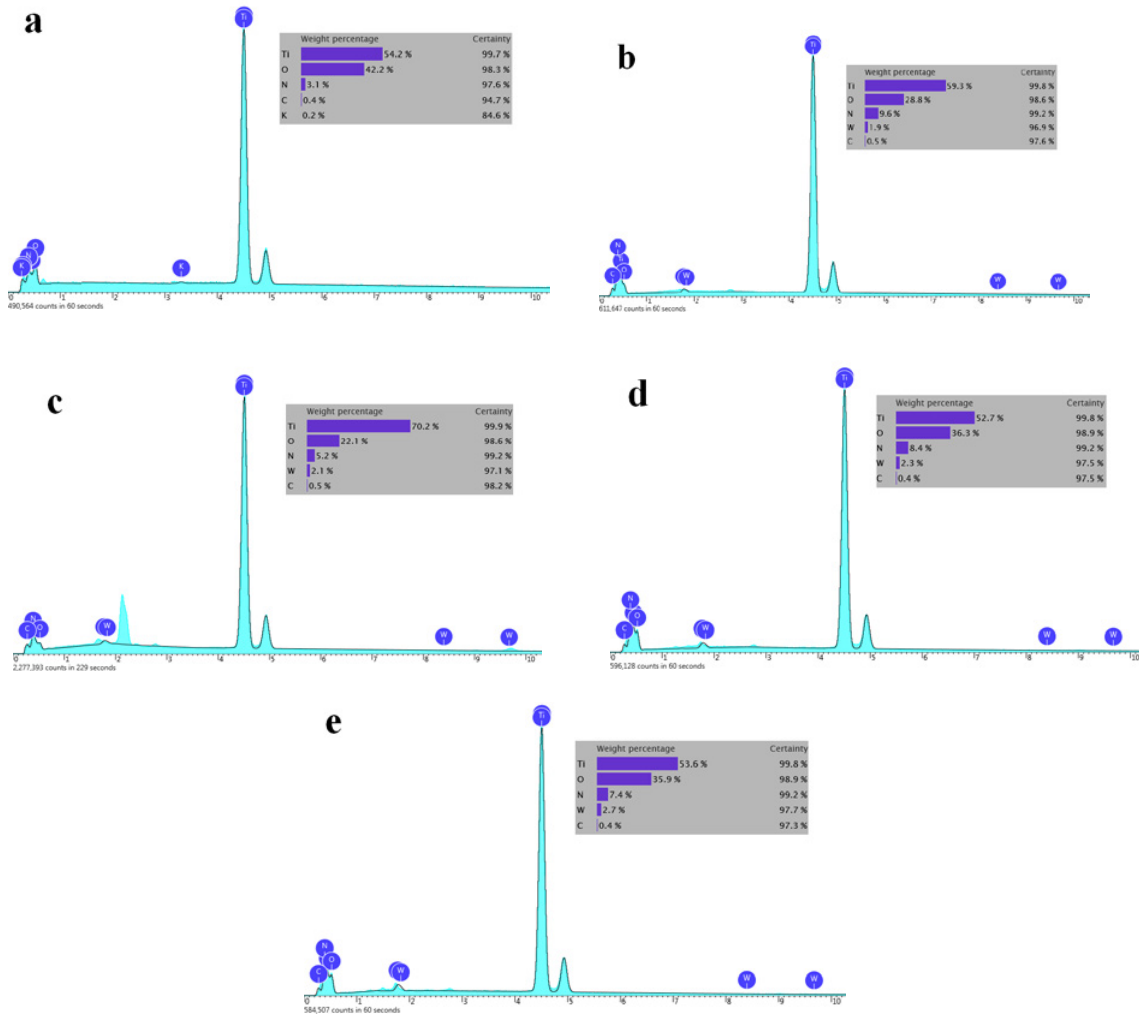


Fig. 5. EDX spectra of different samples; a: Sample A, b: Sample B, c: Sample C, d: Sample D and e: Sample E.

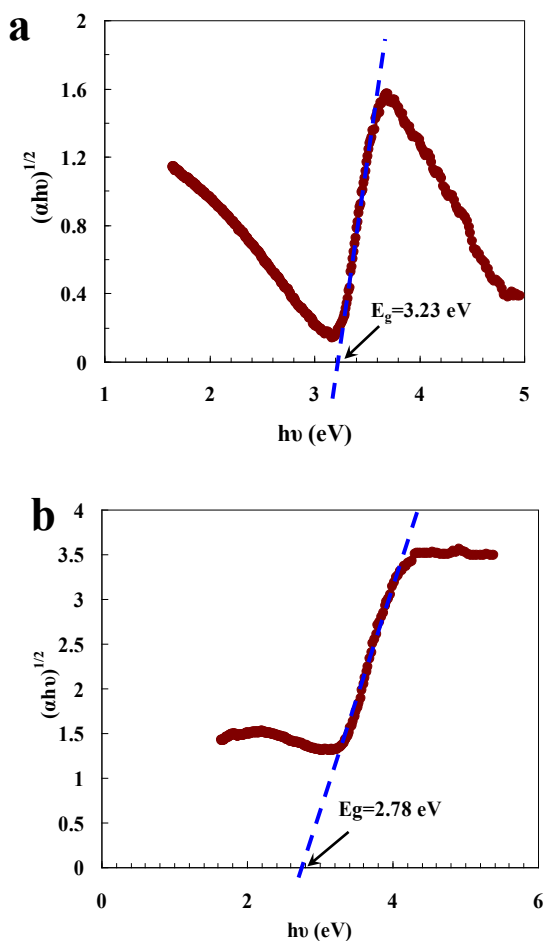


Fig. 6. Plots of $(\alpha h\nu)^{1/2}$ vs. $h\nu$ employed to calculate the band gap value of (a) bare titanium dioxide and (b) titanium dioxide-tungsten trioxide nanocomposite samples.

formation of titanium dioxide-tungsten trioxide nanocomposites film.

Regarding to the UV-Vis spectra recorded data; the absorption edge of sample titanium dioxide-tungsten trioxide nanocomposites was closer to the visible light region than that of bare titanium dioxide. The results obtained have shown that the band gap became narrower and red shifted for nanocomposite films (Fig. 6). The band gap energies decreased progressively from ~ 3.23 eV for bare titanium dioxide to ~ 2.78 eV for titanium dioxide-tungsten trioxide nanocomposites film, according to the equation. These results indicate that the doping of tungsten in titanium dioxide films decreases the band gap.

Photo catalytic activity of different samples was followed through degradation of methylene blue as a function of irradiation time with visible light

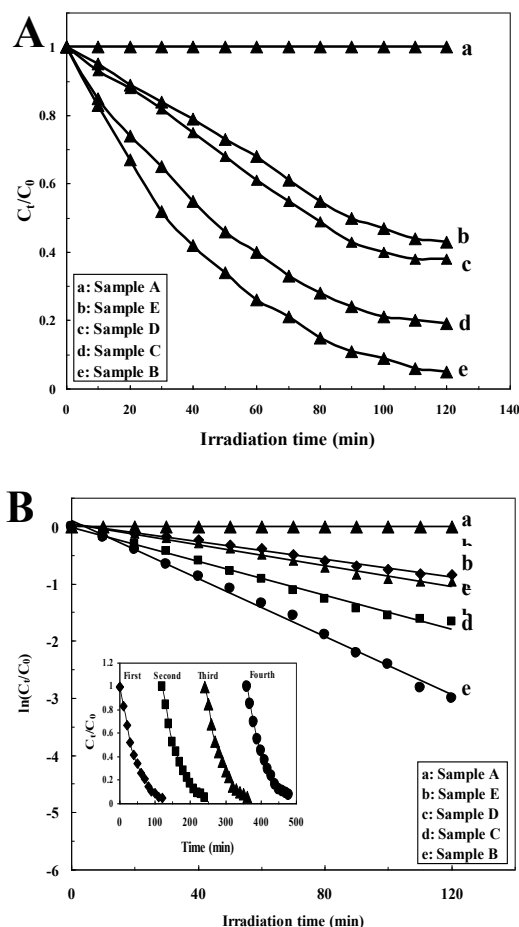


Fig. 7. A: The photo catalytic degradation of methylene blue over the different samples under visible light irradiation. B: $\ln(C_t/C_0)$ vs. irradiation time plot. (Inset) photo catalyst stability test of sample B for photo catalytic degradation of MB.

(Fig. 7). The first, methylene blue degradation experiments were conducted under visible light irradiation to evaluate direct photolysis without the addition of any catalyst. The concentration of methylene blue remained nearly constant after 120 min of irradiation. Thus, no obvious degradation of methylene blue was observed in this time period. In addition, a dark control experiment was conducted, indicating that the adsorption of methylene blue onto the surface of the catalyst in the absence of visible light radiation was negligible. The photo catalysis results indicated that the photo catalytic process was very effective in the removal of methylene blue and it was observed that the degradation of methylene blue was enhanced using titanium dioxide-tungsten trioxide nanocomposite samples. Fig. 7A show photo catalytic activity of different samples that were

Table 2: The apparent first-order rate constant (k) of photo catalytic degradation of methylene blue for different samples.

Samples	Apparent rate constant, k (min^{-1})	Correlation coefficient, R^2
A		
B	2.55×10^{-2}	0.995
C	1.48×10^{-2}	0.990
D	0.90×10^{-2}	0.987
E	0.77×10^{-2}	0.990

followed through degradation of methylene blue as a function of irradiation time with visible light. Under the irradiation of visible light, bare titanium dioxide sample showed almost no photo catalytic activity, but the titanium dioxide-tungsten trioxide nanocomposites samples showed photo catalytic activity. Fig. 7A show that the sample B exhibited better photo catalytic activity than other samples under visible light illumination.

The experimental results of the titanium dioxide photo catalytic degradation of different organic contaminants revealed that the corresponding data fit to the Langmuir-Hinshelwood kinetic model that can be simplified to a pseudo-first-order kinetic equation as follows for diluted solutions [15]:

$$\ln\left(\frac{C_t}{C_0}\right) = -k_{app} t \quad (12)$$

where C_t is the concentration of methylene blue at time t , C_0 is the equilibrium concentration after adsorption and k_{app} is the apparent rate constant. From the plot of $\ln(C_t/C_0)$ vs. irradiation time (Fig. 7B), we can see that the plots represent a straight line and the slope of linear regression can be equal to the apparent first-order rate constant k . The apparent first-order rate constants and correlation coefficients corresponding to Fig. 7B are listed in Table 2. The stability of a photo catalyst was also important to its practical application for it can be regenerated and reused. We investigated the cyclic stability of sample B by monitoring the catalytic activity during successive cycles of use. As shown in Fig. 7B (Inset), after a four-cycle experiment, this catalyst exhibited similar catalytic performance without significant deactivation, revealing its high stability after multiple reuses.

CONCLUSION

The influence of composition electrolyte on the morphology and photo catalytic properties of anodized titanium nanoporous film has been

investigated. An optimum sodium tungstate concentration of 1.2 mM leads to nanostructures films. When sodium tungstate concentration in anodizing solution increased to 1.8 mM, surface is covered with a dense film and then not created any regular nanostructures, implied that composition of anodizing bath is a very important factor in determining the surface and structure of anodized layers. UV-Visible spectroscopy data show that the band gap decrease with increasing sodium tungstate from 3.23 eV for bare titanium dioxide to 2.78 eV for titanium dioxide-tungsten trioxide nanocomposites. Titanium dioxide-tungsten trioxide nanocomposite has excellent photo catalytic performance. The sample B exhibited better photo catalytic activity than other samples. Also this photo catalyst showed good stability and it could be recycled several times without significant loss of its activity. These inexpensive nanocomposite prepared free of noble metals, are interesting candidates to drive photochemical reactions.

ACKNOWLEDGEMENT

The author would like to acknowledge the financial support of Iranian Nanotechnology Society and Isfahan University of Technology (IUT) Research Council.

CONFLICT OF INTEREST

The authors declare that there are no conflicts of interest regarding the publication of this manuscript.

REFERENCES

1. Kang SH, Kim J-Y, Kim HS, Sung Y-E. Formation and mechanistic study of self-ordered TiO₂ nanotubes on Ti substrate. *Journal of Industrial and Engineering Chemistry*. 2008;14(1):52-9.
2. Momeni MM, Nazari Z. Preparation of TiO₂ and WO₃-TiO₂ nanotubes decorated with PbO nanoparticles by chemical bath deposition process: A stable and efficient photo catalyst. *Ceramics International*. 2016;42(7):8691-7.
3. Hamaloğlu KÖ, Çelebi B, Sağ E, Tuncel A. A new method for

- the synthesis of monodisperse-porous titania microbeads by using polymethacrylate microbeads as template. Microporous and Mesoporous Materials. 2015;207:17-26.
4. Momeni MM, Mirhosseini M, Chavoshi M. Growth and characterization of Ta₂O₅ nanorod and WTa₂O₅ nanowire films on the tantalum substrates by a facile one-step hydrothermal method. Ceramics International. 2016;42(7):9133-8.
 5. Mali SS, Shinde PS, Betty CA, Bhosale PN, Lee WJ, Patil PS. Nanocoral architecture of TiO₂ by hydrothermal process: Synthesis and characterization. Applied Surface Science. 2011;257(23):9737-46.
 6. Momeni MM, Ghayeb Y. Cobalt modified tungsten–titania nanotube composite photoanodes for photoelectrochemical solar water splitting. Journal of Materials Science: Materials in Electronics. 2015;27(4):3318-27.
 7. Huang M, Yu J, Li B, Deng C, Wang L, Wu W, et al. Intergrowth and coexistence effects of TiO₂–SnO₂ nanocomposite with excellent photocatalytic activity. Journal of Alloys and Compounds. 2015;629:55-61.
 8. Momeni MM, Ghayeb Y. Photoelectrochemical water splitting on chromium-doped titanium dioxide nanotube photoanodes prepared by single-step anodizing. Journal of Alloys and Compounds. 2015;637:393-400.
 9. Zheng X, Li D, Li X, Chen J, Cao C, Fang J, et al. Construction of ZnO/TiO₂ photonic crystal heterostructures for enhanced photocatalytic properties. Applied Catalysis B: Environmental. 2015;168-169:408-15.
 10. Iliev V, Tomova D, Bilyarska L, Tyuliev G. Influence of the size of gold nanoparticles deposited on TiO₂ upon the photocatalytic destruction of oxalic acid. Journal of Molecular Catalysis A: Chemical. 2007;263(1-2):32-8.
 11. Iliev V, Tomova D, Rakovsky S, Eliyas A, Puma GL. Enhancement of photocatalytic oxidation of oxalic acid by gold modified WO₃/TiO₂ photocatalysts under UV and visible light irradiation. Journal of Molecular Catalysis A: Chemical. 2010;327(1-2):51-7.
 12. Ye M, Gong J, Lai Y, Lin C, Lin Z. High-Efficiency Photoelectrocatalytic Hydrogen Generation Enabled by Palladium Quantum Dots-Sensitized TiO₂ Nanotube Arrays. Journal of the American Chemical Society. 2012;134(38):15720-3.
 13. Iliev V, Tomova D, Todorovska R, Oliver D, Petrov L, Todorovsky D, et al. Photocatalytic properties of TiO₂ modified with gold nanoparticles in the degradation of oxalic acid in aqueous solution. Applied Catalysis A: General. 2006;313(2):115-21.
 14. Puddu V, Mokaya R, Li Puma G. Novel one step hydrothermal synthesis of TiO₂/WO₃ nanocomposites with enhanced photocatalytic activity. Chemical Communications. 2007(45):4749.
 15. Momeni MM, Mirhosseini M, Chavoshi M, Hakimizade A. The effect of anodizing voltage on morphology and photocatalytic activity of tantalum oxide nanostructure. Journal of Materials Science: Materials in Electronics. 2015;27(4):3941-7.